J Mater Sci: Mater Med (2009) 20:257–263
DOI 10.1007/s10856-008-3574-3

Nanoscale viscoelastic properties of an aligned collagen scaffold

Bill Chaudhry · Holly Ashton · Arif Muhamed · Michael Yost · Steve Bull · Daniel Frankel

Received: 14 June 2008 / Accepted: 18 August 2008 / Published online: 3 September 2008

Abstract Localised mechanical properties for aligned collagen scaffolds derived from Type 1 collagen were determined by application of nanoindentation based techniques. It was possible to measure the modulus and hardness with nanometre control over the depth of penetration and quasi-static testing under displacement control yielded average modulus values ranging from 1.71 GPa to 3.31 GPa; a narrower range of values than obtained by other methods. Hardness values of 222 MPa to 256 MPa were recorded and showed little scatter, highlighting the potential of nanoindentation hardness values as a reproducible and accurate measure of soft material properties. Open loop Load-displacement curves for the collagen exhibited the expected shapes for a viscoelastic material and it was thus possible to apply dynamic stiffness measurement at the nano scale. As well as determining the storage modulus (0.71 GPa) and the loss modulus (0.40 GPa) at the sub-micron length and nano depth resolution it was also possible to discriminate between surface and bulk readings allowing surface effects to be discarded if necessary. In addition to being a more accurate indentation method than atomic force microscopy, the localised dynamic mechanical properties of collagen were measured for the first time. These results demonstrate that this nanoindentation technique can serve as a powerful tool for the characterisation of collagen based biomaterials that are used as scaffolds for a variety of engineered tissues, such as artificial skin, skeletal muscle, heart valves and neuroregeneration guides.

B. Chaudhry
Institute of Human Genetics, Newcastle University, Newcastle upon Tyne NE1 3BZ, UK

H. Ashton · A. Muhamed · S. Bull · D. Frankel (✉)
School of Chemical Engineering and Advanced Materials, Newcastle University, Newcastle upon Tyne NE1 7RU, UK
e-mail: d.j.frankel@ncl.ac.uk

M. Yost
Department of Surgery, School of Medicine, University of South Carolina, Columbia, SC 29208, USA

1 Introduction

Collagen based biomaterials are increasingly used to construct tissue engineering scaffolds and have found diverse applications that include production of artificial skin, skeletal muscle, cardiac valves and neuroregeneration guides for severed nerves [1–4]. Most applications require the scaffold to operate under mechanical stresses and thus the behaviour of collagen under applied force is a crucial consideration in tissue engineering design [5, 6]. A further factor complicating the structural characteristics of collagen and consequently its performance in vivo is the wide variety of manufacturing processes that produce variation in the degree of fibre alignment, cross linking and form. Thus, manufacturing processes such as solid freeform fabrication [7], electro spinning [8] and extrusion [9] have been developed for specific biomaterial applications and although all products may be composed of the same collagen structural material, the mechanical properties may differ due to their processing method.

Previous studies have measured the wet and dry mechanical properties of collagen in natural forms, for example such as in tendons, or in artificial states as seen with collagen gels. For example, conventional macroscopic mechanical testing procedures were applied to collagen scaffolds and fibres by Gentleman et al. and stress-strain

curves obtained [10]. At a higher level of spatial resolution Wang et al. used micro tensile testing to measure the mechanical properties of collagen fibrils [11]. They were able to tease the collagen fibrils apart using a tensile test system with 50 nN load resolution. At the nanoscale Mesquida et al. measured the mechanical properties of collagen fibres with atomic force microscopy (AFM) both by application of tension to fibres attached between the tip and the plate surface as well as by using the AFM tip as an indenter [12]. They measured a range of modulus values between 5 GPa and 11.5 GPa. Yang et al. have pioneered the use of micropatterned surfaces for measuring the bending behaviour of single collagen fibrils by bridging fibres across the channels and using an AFM tip to produce localised deformation [13, 14].

Collagen is a viscoelastic material and shows time dependent behaviour including creep and stress relaxation. Indeed many of the biological roles performed by collagens make use of these phenomena, for example the dissipation of stress within the Achilles tendon during heel strike. These viscoelastic properties are normally only measured in the macroscopic bulk condition using rheometry or dynamic mechanical analysis [15, 16]. As a consequence of these mechanical considerations and the effects of the arrangement of molecules/fibrils and fibres into a three dimensional material it is usual to characterise collagen at the molecular or fibrillar level [17, 18].

Although atomic force microscopy (AFM) has lent itself to the study of such systems due to its nanometre resolution in terms of lateral/vertical position, there are several drawbacks to the application of AFM for the nanomechanical properties of collagen by indentation. In measuring Young's Modulus (E), knowledge of the contact area of the tip with the surface is required. Unfortunately the AFM tip shape and size can only be estimated and thus the calculated values for applied stress cannot be determined with certainty. Moreover, the AFM tip does not approach the material surface vertically but engages in an arc further complicating the calculation of applied stress. Nanoindentation inherently overcomes these problems as the surface area of the probe can be determined and applied in a vertical plane. In addition, the dynamic mode permits the measurement of localised viscoelastic properties [19–21]. In comparison to conventional hardness tests, which are essentially macroscopic, nanoindentation allows the local properties of sub-micron regions to be explored without being averaged out. This information is particularly important when dealing with scaffolds manufactured from biomaterials such as collagen which may have non-homogenous properties at this resolution scale of relevance to cellular behaviours. For example, aligned spun collagen type 1 tubing [22] has been shown to support in vivo type cardiomyocyte differentiation with organised contractile arrays, intercellular connections and spontaneous contraction, in contrast to the appearance of non-differentiated and non-contractile cardiomyocytes when the same cells are grown on collagen coated rigid plates.

2 Materials and methods

2.1 Fabrication of collagen tube

The manufacture of tubes from collagen fibres has been developed by Yost et al. [11]. In summary, bovine type one collagen extracted from cowhide was fed into an apparatus consisting of counterrotating cones and extruded into an atmosphere of air containing anhydrous ammonia to aid collagen polymerisation. Following this the tubing was treated in water and sodium hydrogen carbonate. The outer diameter of the tube obtained was 5 mm and the inner diameter 4 mm. For nanoindentation measurement the tubes were cut into rectangular pieces and mounted on an aluminium stub using superglue. Samples were left to dry for up to 24 h to allow for dehydration.

2.2 Quasi static nanoindentation

Quasistatic nanoindentation measurements were performed with a Hysitron Triboindenter utilising a Berkovich diamond tip (radius of curvature 100 nm). A schematic of the setup is shown in (Fig. 1a). The indentor tip is mounted on the middle plate of a three plate capacitor which is used for both displacement sensing and application of the load (direct current bias applied to the bottom plate of capacitor). High resolution positioning of the tip is achieved using a piezoelectric scanner. The scanner is also used to engage with the surface. Corrections are made for the thermal drift of this element. Temperature of the enclosure was maintained to plus or minus 0.1°C and an active damping

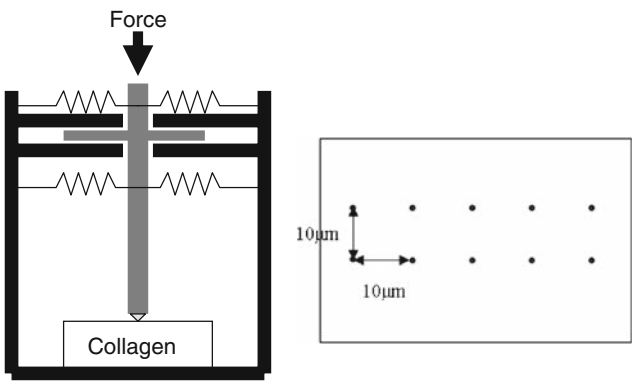

Fig. 1 **(a)** Schematic of 3 plate nanoindenter. **(b)** 10 point grid with each point seperated by 10 μm. A force displacement curve was taken at each point on the grid

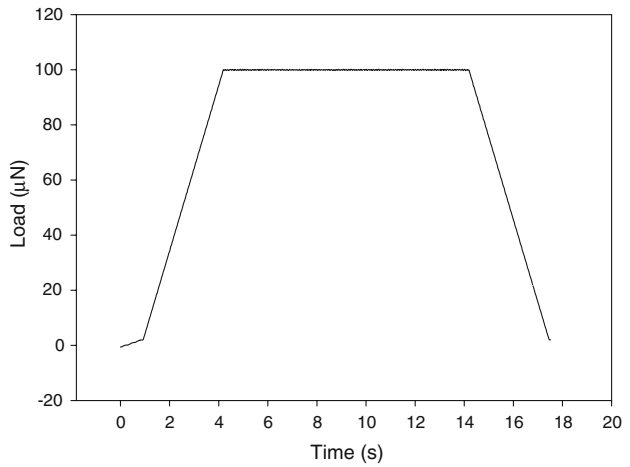

Fig. 2 A trapezoidal load function applied for quasi-static nanoindentation of collagen substrates. In this case the maximum load of 100 μN was held for 10 s. Loading and unloading rate was 30 μN/s

system was used to minimise the effects of vibration. Indents were recorded in a pre determined rectangular grid at ten points, each separated by 10 μm (Fig 1b). The load profile was selected so that the loading and unloading rate was 30 μN/s and the maximum load was held for 10 s (Fig. 2).

Using a method developed by Oliver and Pharr [23] the hardness H, and the reduced modulus E_r (the combined modulus of the tip and sample) can be directly determined from the analysis of the load displacement data using Eqs. 1 and 2.

$$E_r = \frac{S_u}{2}\sqrt{\frac{\pi}{A}} \tag{1}$$

$$H = \frac{P_{\max}}{A_C} \tag{2}$$

Where S_u is the initial unloading stiffness (the slope of the unloading curve dP/dh, evaluated at the maximum load), $P_{\max}$ is the maximum load applied during indentation, A_c is the contact area at the indenter tip and the sample. The value A_c can be calculated from the contact depth, h_c, which is the depth of the impression in the absence of the elastic depression of the test surface. By the addition of h_c, and the elastic depth, h_{elas}, a value for the total indenter penetration depth is recorded by the transducer giving Eq. 3.

$$h_f = h_c + h_{\text{elas}} \tag{3}$$

In turn the value of $h_{\max}$ can be calculated using Eq. 4,

$$h_{\text{elas}} = \frac{\varepsilon P}{S_U} \tag{4}$$

Where, ε is the constant that depends on the indenter geometry. For the tests conducted in this paper a Berkovich tip was used giving a ε value of 0.75. Applying Eqs. 3 and 4 h_C can then be calculated and from this the contact area A_c can be derived.

$$A_C = 24.5h_C^2 \tag{5}$$

The reduced modulus E_r relates to the sample modulus by rearrangement of Eq. 6,

$$\frac{1}{E_r} = \frac{\left(1-v_S^2\right)}{E_S} + \frac{\left(1-v_i^2\right)}{E_i} \tag{6}$$

Where the subscripts s and i refer to the sample and indenter moduli respectively, v is the Poisson's ratio. The properties of the indenter tip are determined prior to testing of the material. The indenter tip will always have a Young's modulus very much higher than that of the specimen to achieve accurate results for the sample tested. From this the Young's modulus for the material can be calculated if the Poisson's ratio for the sample is known. When the Poisson's ratio is unknown for the material the plane strain modulus may be cited instead.

$P_{\max}$ and S_u can be determined by analysis of the load displacement data. The projected contact area at maximum load A_c, is determined by a premeasured tip area function. The function was determined by calibrating the indenter, by using the method of Oliver and Pharr [23]. This provides a method of calibration using indentation tests made in fused silica which is elastically isotropic and can be assumed to have a constant Young's modulus with depth.

2.3 Nanoscale dynamic mechanical analysis

Dynamic mechanical behaviour was measured on the Hysitron Triboindenter by superimposing a sinusoidal stress to the specimen with an alternating current signal onto the direct current signal responsible for loading the sample. In a viscoelastic material the strain lags behind the applied stress during cyclic loading. The applied sinusoidal strain and stress, Fig. 3a can be represented mathematically as

$$\varepsilon = \varepsilon_0 \sin \omega t \tag{7}$$

$$\sigma = \sigma_0 \sin(\omega t + \delta) \tag{8}$$

Where ε is the strain, ε_0 the strain amplitude, σ the stress and σ_0 the stress amplitude. δ is the phase lag. Eq. 8 can be expanded to

$$\sigma = \sigma_0 \sin(\omega t)\cos\delta + \sigma_0 \cos(\omega t)\sin\delta \tag{9}$$

Hence the stress can be considered as being resolved into two components. One which is in phase and another which is 90° out of phase with the strain. This is best represented diagrammatically Fig. 3b. Consider two rotating vectors of magnitude σ_0 and ε_0 with a phase difference δ. It follows

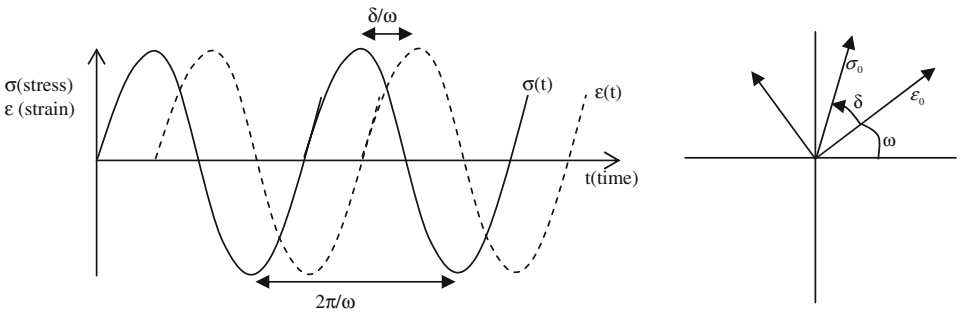

Fig. 3 **(a)** Sinusoidal loading of a viscoelastic material with the strain response lagging behind the stress. **(b)** Vectorial representation of the cyclic loading behaviour

that we can define two moduli one in phase and one out of phase.

$$E_1 = \frac{\sigma_0 \cos \delta}{\varepsilon_0} \tag{10}$$

$$E_2 = \frac{\sigma_0 \sin \delta}{\varepsilon_0} \tag{11}$$

Therefore

$$\tan \delta = \frac{E_2}{E_1} \tag{12}$$

E_1 is the "storage modulus" and defines the elastically stored energy. E_2 is the "loss modulus" and relates to the energy lost during a cycle.

The indenter head was first calibrated prior to each test in air in order to determine the head dynamics which need to be subtracted from the measured data to determine the sample response. A frequency of 10 Hz was used for testing and the storage and loss moduli were recorded at 15 points for each indentation.

3 Results

3.1 Quasi static nanoindentation results

Figure 4 shows a typical force distance curve for a loading profile with peak load of 200 μN. The curve takes the typical form for a viscoelastic material. In particular the collagen exhibits the viscoelastic phenomenon of creep, that is as the load is held constant at 200 μN, the material continues to deform. Moreover clear hysteresis is apparent as after the load is removed the deformation is far from recovered. This measurement in itself is significant as the viscoelastic character of the collagen scaffold has been recorded with a z resolution of nanometres. All curves taken showed exactly the same viscoelastic form. A typical collagen fibril has a diameter between 50–200 nm and thus we are able to interrogate the mechanical behaviour at the fibril length scale although in lateral terms stress will have been applied to several fibrils. By increasing the load it is possible to penetrate deeper into the material and thus

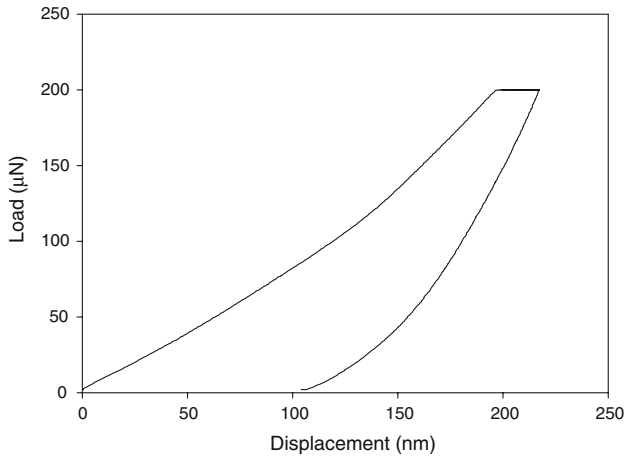

Fig. 4 A typical load/displacement curve for the collagen scaffold taken under quasi static conditions with a maximum load of 200 μN. All curves taken were of the same form. The curve takes the classic form for a viscoelastic material exhibiting both creep and hysteresis

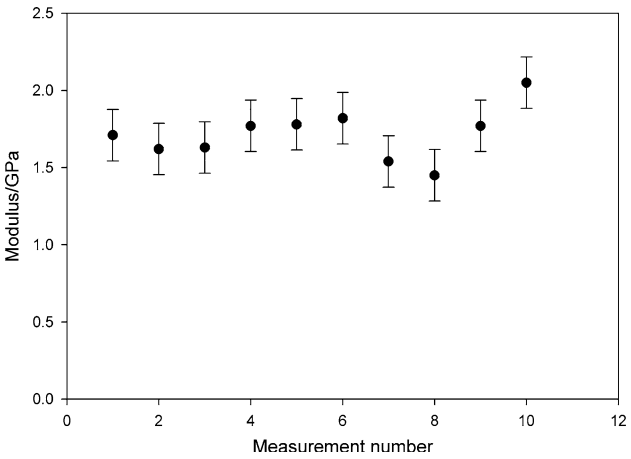

Fig. 5 Modulus value distribution over ten test points of experimental grid. Error bars are standard deviations

mechanical properties which could change discretely with depth can be investigated.

The modulus and hardness values were calculated for each of the ten curves taken during a single test. A typical distribution of modulus values over the ten test points is shown in Fig. 5 for the experiment with maximum load of

150 μN. There was no correlation between modulus and increasing load and thus in the case of quasistatic nanoindentation surface effects do not appear to play a significant role. Modulus values ranged from 1.71 GPa to 3.31 GPa. These values are lower than those recorded by Mesquida et al. [12] who measured a range of values of between 5 GPa to 11.5 GPa for the moduli of single collagen fibrils by AFM based nanoindentation. The range of values measured in our study is much narrower and this improved reproducibility may be attributed to greater accuracy using this technique over AFM. Unlike the AFM based nanoindentation study it was not necessary to approximate the shape/size of the tip and there was no need to compensate for a non vertical approach.

Hardness values were between 222 MPa and 256 MPa and the scatter within one set of experiments is presented in Fig. 6. To our knowledge hardness values have not previously been reported for collagen so these values are of particular interest.

3.2 Dynamic stiffness measurements

The dynamic mechanical stiffness measurements made it possible for us to formally assess the viscoelastic mechanical properties of the collagen. We were able to measure the storage modulus, loss modulus and tan delta at high resolution. Indeed the ability to take measurements as different depths below the surface of the collagen allowed us to build a depth profile of the biomaterial. The data demonstrated a storage modulus of $E' = 2.82\text{GPa}$ and loss modulus $E'' = 0.39\text{GPa}$ at the surface of collagen scaffolds that had been left to dry in air for 24 h. It is possible to validate these values with the relationship between modulus, storage modulus and loss modulus. In complex notation:

$$E = E_1 + \mathrm{i}E_2 \tag{13}$$

$$|E| = \sqrt{E_1^2 + E_2^2} \tag{14}$$

In this case it seemed apparent that the storage modulus was very close to the actual modulus indicating that the collagen exhibited elastic rather than viscoelastic properties. However further values were measured at increasing penetration depths and, for every curve recorded, a decrease in storage modulus resulted with increasing depth. If continued this would finally lead to a plateau in which the storage modulus would level out. Such a decrease in storage modulus with depth is a common observation with nanoindentation and results from the difference in properties between the surface and the bulk of a material. This effect, sometimes called the indentation size effect, has been widely reported for metals and ceramics but the results here demonstrate that it is equally important in polymers and biomaterials (Fig. 7).

4 Discussion

At this point it is pertinent to discuss the difference between hardness and modulus in addition to describing where a knowledge of the hardness of collagen biomaterials at the nanoscale would be useful. Both the hardness and elastic modulus of a material can be anisotropic at short length scales but most modulus measurement techniques (including indentation) sample the elastic properties over larger length scales. However, nanoindentation is ideally placed to determine localised variations in hardness. Hardness represents a materials ability to resist permanent deformation, and in applications where collagen biomaterials change over time, for example due to degradation or biological interactions, hardness could be crucial

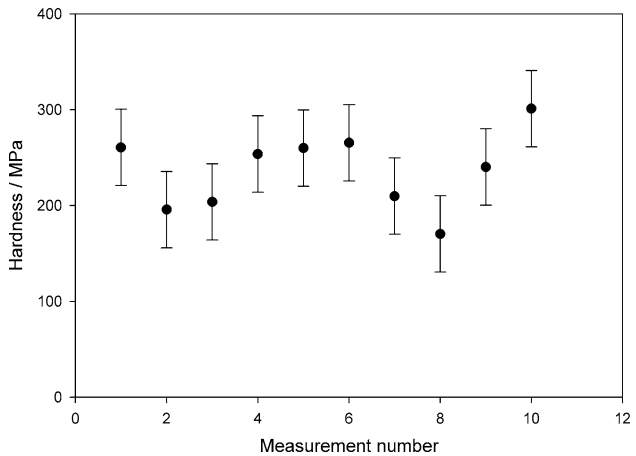

Fig. 6 Hardness value distribution over ten test points of experimental grid. Error bars are standard deviations

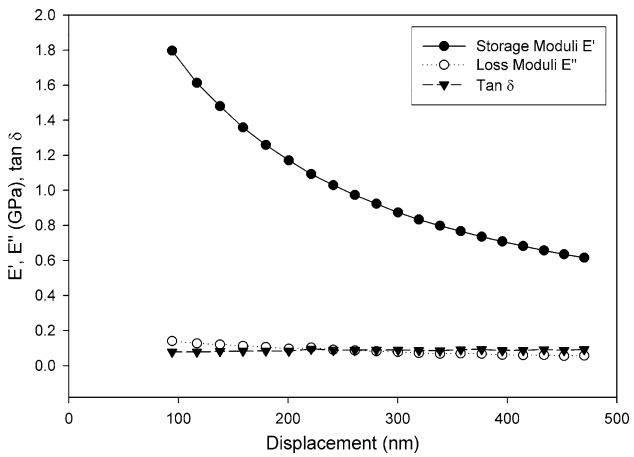

Fig. 7 Variation of storage modulus, lost modulus and tan delta with penetration depth into the collagen scaffold

in designing for long term performance. It was also noted that the hardness values show far less scatter within a set of ten measurements and from sample to sample than modulus values. This is because most of the instrumental error derives from uncertainties in position measurement. Unlike the modulus, the hardness is related to the distance measured as displacement squared, therefore squaring of fractional displacement uncertainties leads to smaller errors. We suggest that hardness measurements may be more appropriate for the evaluation of mechanical properties of collagen at these length scales. It is important to point out that for viscoelastic materials the Oliver and Pharr analysis breaks down. However in this study the effects of viscoelasticity on the results were minimised. This was achieved by loading quickly and minimising the total test time. Moreover the amount of viscoelasticity exhibited in the load hold time was limited as the contact pressure was kept as small as possible to aid in obtaining reliable data. There was little evidence of viscoelastic recovery of the indent at the end of the unloading cycle. An additional validation of the quasi static Oliver and Pharr analysis was the consistency of data with the storage and loss moduli (obtained through dynamic stiffness measurements) calculated using Eq. 15.

An interesting comparison of the nanoscale dynamic stiffness measurements are to the bulk dynamic mechanical analysis of mouse tail collagen measured by Ntim et al. [24] as they were looking at the effect of hydration state on collagen mechanical properties. Tan delta values obtained in this study representing the phase lag between applied stress and strain response ranged between 0.2 and 0.4 as did the tan delta values for the bulk collagen derived from mouse tail.

In terms of accuracy roughness of a surface will affect the actual contact area with a probe and thus will alter the values of mechanical properties calculated through contact mechanics. The presented technique allows the surface related artefacts to be followed and if need be ignored by profiling the changes with depth. It is therefore possible to take the constant value at the plateau as the measurement which is unaffected by both surface phenomenon and surface related artefacts. In the case of the aligned collagen scaffold it took about 500 nm of penetration before the storage modulus reached a plateau and led to storage modulus values of 0.70 GPa.

With regards to hydration states affecting mechanical properties, the nanoindentation experiments were performed on several samples which were allowed to dry for either 4, 24 or 48 h. Results did not seem to depend on time left to dry and most probably as Mesquida concluded drying was only a surface phenomenon with most of the water still trapped in the collagen structure. These dehydration variations would have been incorporated into the previously discussed scatter in the data.

Another contributing factor to the accuracy of the measured values is the tip area calibration procedure. In the case of AFM, the main technique that has been used to calculate nanoscale mechanical properties of collagen, the tip size is given a nominal value and the shape is unknown. This has lead to large inaccuracies in subsequent contact mechanics calculations [25]. With nanoindentation the tip area calibration goes some way towards solving this problem.

Bulk measurement techniques such as conventional indentation and dynamic mechanical analysis are not sensitive to the microstructural complexity of a biomaterial and only report average values. However with nano and microstructured natural biomaterials (a consequence of hierarchical self assembly) these local variations are important to probe. For synthetic soft biomaterials such variations are equally relevant as the surface plays a crucial role in the immune response and in biological integration.

5 Conclusion

It has been demonstrated that the mechanical properties of a collagen biomaterial can be measured with high accuracy as a function of depth at the nanometre level. It was also shown that hardness values have less scatter than modulus values and thus may be a better measure of collagen mechanical properties. Dynamic stiffness measurements revealed values for storage and loss modulus as a function of penetration depth. It was apparent that storage modulus decreased with indentation depth which was attributed to both surface effects and surface inaccuracies related to tip/area calibration. A value of 0.70 GPa at 500 nm indentation depth instead of 2.82 GPa at the surface was taken as representative of the materials storage modulus. In conclusion it has been demonstrated that nanoindentation can measure the nanoscale viscoelastic properties of collagen, that it has the ability to measure mechanical property changes with depth at the nanometre resolution for soft biomaterials and that the technique has the potential application for studying inhomogeneous features in biomaterials. It is also apparent that this technique yields a narrower range of modulus values than atomic force microscopy, a fact that can be attributed to the superior accuracy of the technique for this type of measurement.

Acknowledgement D.J. Frankel is supported by a Research Councils UK (RCUK) fellowship.

References

1. Q. Lu, K. Ganesan, D.T. Simionescu, N.R. Vyavahare, Biomaterials **25**, 5227 (2004). doi:10.1016/j.biomaterials.2003.12.019

2. P.M. Taylor, A.E.G. Cassl, M.H. Yacoub, Prog. Pediatr. Cardiol. **21**, 219 (2006). doi:10.1016/j.ppedcard.2005.11.010
3. J.T. Lu, C.J. Lee, S.F. Bent, H.A. Fishman, E.E. Sabelman, Biomaterials **28**, 1486 (2007). doi:10.1016/j.biomaterials.2006.11.023
4. M.T. Valarmathi, M.J. Yost, R.L. Goodwin, J.D. Potts, *Tissue Eng: Part A* **14** (2008)
5. R.G. Jansen, T.H. van Kuppervelt, W.F. Daamen, A.M. Kuijpers-Jagtman, W. Von den Hoff, Arch. Oral. Biol. **53**, 376 (2008)
6. V. Thomas, X. Zhang, S.A. Catledge, Y.K. Vohra, Biomed. Mater. **2**, 224 (2007). doi:10.1088/1748-6041/2/4/004
7. E. Sachlos, N. Reis, C. Ainsley, B. Derby, J.T. Czernuszka, Biomaterials **24**, 1487 (2003). doi:10.1016/S0142-9612(02)00528-8
8. L. Buttafoco, N.G. Kolkman, P. Engbers-Buijtenhuijs, A.A. Poot, P.J. Dijkstra, I. Vermes, Biomaterials **27**, 724 (2006). doi:10.1016/j.biomaterials.2005.06.024
9. M. Rafiuddin Ahmed, U. Venkateshwarlu, R. Jayakumar, Biomaterials **25**, 2585 (2004). doi:10.1016/j.biomaterials.2003.09.075
10. E. Gentleman, A.N. Lay, D.A. Dickerson, E.A. Nauman, G.A. Livesay, K.C. Dee, Biomaterials **24**, 3805 (2003). doi:10.1016/S0142-9612(03)00206-0
11. X. Wang, X. Li, M.J. Yost, J. Biomed. Res. Part A **74A**, 263 (2005). doi:10.1002/jbm.a.30387
12. M.P.E. Wenger, L. Bozec, M.A. Horton, P. Mesquida, Biophys. J. **93**, 1255 (2007). doi:10.1529/biophysj.106.103192
13. L. Yang, C.F.C. Fitie, K.O. Van Der Werf, M.L. Bennink, P.J. Dijkstra, J. Feijen, Biomaterials **29**, 955 (2008). doi:10.1016/j.biomaterials.2007.10.058
14. L. Yang, K.O. Van der Werf, B.F.J.M. Koopman, V. Subramaniam, M.L. Bennink, P.J. Dijkstra, J. Biomed. Res. Part A **82A**, 160 (2007). doi:10.1002/jbm.a.31127
15. G. Forgacs, S.A. Newman, B. Hinner, C.W. Maier, E. Sackmann, Biophys. J. **84**, 1272 (2003)
16. P. Netti, A. D'amore, D. Ronca, L. Ambrosio, L. Nicolais, J. Mater. Sci. Mater. Med. **7**, 525 (1996). doi:10.1007/BF00122175
17. L. Bozec, M. Horton, Biophys. J. **88**, 4223 (2005). doi:10.1529/biophysj.104.055228
18. M.J. Buehler, Proc. Natl. Acad. Sci. USA **103**, 12285 (2006). doi:10.1073/pnas.0603216103
19. A. Chakravartula, K. Komvopoulos, Appl. Phys. Lett. **88**, 131901 (2006). doi:10.1063/1.2189156
20. S.J. Bull, J. Appl. Phys. D **38**, R393 (2005). doi:10.1088/0022-3727/38/24/R01
21. N. Bouaita, S.J. Bull, J. Fernandez Palacio, J.R. White, Polym. Eng. Sci. **46**, 1160 (2006)
22. H.J. Evans, J.K. Sweet, R.L. Price, M. Yost, R.L. Goodwin, Am. J. Physiol. Heart Circ. Physiol. **285**, H570 (2003)
23. W.C. Oliver, G.M. Pharr, J. Mater. Res. **7**, 1564 (1992). doi:10.1557/JMR.1992.1564
24. N.M. Ntim, A.K. Bembey, V.L. Ferguson, A.J. Bushby, Mater. Res. Soc. Symp. Proc. **898**, L05 (2006)
25. C.A. Clifford, M.P. Seah, Appl. Surf. Sci. **252**, 1915 (2005). doi:10.1016/j.apsusc.2005.08.090